

RSC Advances



This is an *Accepted Manuscript*, which has been through the Royal Society of Chemistry peer review process and has been accepted for publication.

Accepted Manuscripts are published online shortly after acceptance, before technical editing, formatting and proof reading. Using this free service, authors can make their results available to the community, in citable form, before we publish the edited article. This *Accepted Manuscript* will be replaced by the edited, formatted and paginated article as soon as this is available.

You can find more information about *Accepted Manuscripts* in the [Information for Authors](#).

Please note that technical editing may introduce minor changes to the text and/or graphics, which may alter content. The journal's standard [Terms & Conditions](#) and the [Ethical guidelines](#) still apply. In no event shall the Royal Society of Chemistry be held responsible for any errors or omissions in this *Accepted Manuscript* or any consequences arising from the use of any information it contains.

Local electric field factors by a combined charge-transfer and point-dipole interaction model[†]

Nazanin Davari,^a Shokouh Haghdani,^a Per-Olof Åstrand ^{*a} and George C. Schatz ^b

Received Xth XXXXXXXXXXXX 20XX, Accepted Xth XXXXXXXXXXXX 20XX

First published on the web Xth XXXXXXXXXXXX 200X

DOI: 10.1039/b000000x

A force-field model for the local electric field as a linear response to a frequency-dependent external electric field is presented based on a combined charge-transfer and point-dipole interaction (CT-PDI) force-field model for frequencies through the first absorption maximum. The local electric field provides a measure of the mutual interactions of the molecules with each other, as is important in problems ranging from dielectric breakdown to solvent polarization and energy transfer. It also indicates how resonant excitation of these molecules can perturb Raman scattering by a third molecule located nearby through an intensity borrowing mechanism. The CT-PDI model is a combination of a modified electronegativity equalization model including non-metallic behaviour and a point-dipole interaction model described by atomic polarizabilities which also includes the time-dependence of the atomic charges and atomic dipole moments. A parametrization of frequency-dependent polarizabilities through the first absorption maximum calculated by time-dependent density-functional theory has been extended for a set of hydrocarbon and azobenzene molecules to provide atom-type parameters for the CT-PDI model. As initial model systems, results are presented for the benzene and azobenzene dimers for the local electric field response at points between the molecules and at the atoms in the molecules. As expected, the response depends critically on the intermolecular distance between the monomers. The azobenzene dimer shows a larger local field response at the atoms in the phenyl rings compared to the benzene dimer and the response at the nitrogen atoms is larger than at the hydrogen and carbon atoms in the azobenzene dimer, which can be rationalized qualitatively by that the charge and dipole contributions to the local field factor either add up or to a large extent cancel each other. At the absorption frequency, the largest local field factor of the benzene dimer is around 6 and for the azobenzene dimer it is around 12, respectively, at typical distances indicating that the response may be significant.

1 Introduction

In an external electric field, the molecules in a dielectric liquid are polarized resulting in a local electric field at the molecule which is different from the external electric field. The local electric field is a sum of the external electric field and the electric field of the permanent and induced multipole moments established in the presence of the external electric field.^{1–3} The Lorentz approach⁴ has been used frequently as an approximate method to determine the local electric field. In this approach, the local field at a certain point of a dielectric is the same as that inside a fictive sphere. However, the Lorentz model is limited to non-polar materials and it is assumed that the contribution of electric dipoles inside the sphere is zero. Polarization from an atomistic point of view requires knowledge of the local field at the atoms of the dielectric as a re-

sponse to an external electric field.

Quantum chemical response theory⁵ and time-dependent density-functional response theory (TDDFT)⁶ are standard methods to obtain response properties for small and medium-sized systems. Electric dipole shieldings and hypershieldings⁷ have been calculated at the Hartree-Fock level of theory^{8–10} which determine the linear and non-linear local field responses to the external field. In TDDFT calculations, the accuracy of the response properties depends critically on the choice of density functionals,^{11–15} because the exchange-correlation potential in approximate standard functionals shows incorrect asymptotic decay of the true electrostatic potential.^{16,17} Long-ranged corrected (LC) functionals with the correct asymptotic behaviour have been suggested as alternatives for this purpose.^{18–23}

Force-field models have been used as an alternative for the calculation of response properties of relatively large molecules. The point-dipole interaction (PDI) model,^{24–28} has been used for the calculation of the polarizabilities of carbon nanotubes and fullerenes,^{29–34} boron nitride tubes³⁵ and proteins,³⁶ and it has also been extended to properties like optical rotation^{37–40} and hyperpolarizabilities.^{30,31,33,41–45} In the

[†] Electronic Supplementary Information (ESI) available: [details of any supplementary information available should be included here]. See DOI: 10.1039/b000000x/

^a Department of Chemistry, Norwegian University of Science and Technology (NTNU), NO-7491, Trondheim, Norway. E-mail: per-olof.aastrand@ntnu.no

^b Department of Chemistry, Northwestern University, 2145 Sheridan Road, Evanston, IL 60208-3113, USA.

PDI model, atomic polarizabilities couple with each other in an external electric field through the atomic induced dipole moments and the molecular polarizability is obtained by considering atomic polarizabilities as atom-type parameters.

To calculate atomic charges, the electronegativity equalization model (EEM)^{46–48} has been used where the charge-transfer between atoms is calculated by atomic electronegativities and chemical hardnesses as atom-type parameters. To resolve the limitation of the EEM regarding the charge transfer over large distances,^{49,50} the atom-atom charge-transfer (AACT) method⁴⁹ is adopted in a model that is transferable to both metallic and non-metallic systems.^{51–57} In a metallic model like EEM, charges are allowed to move without a significant resistance between the atoms such as in highly conjugated systems, while a non-metallic model describes molecules with much less charge-transfer as for example in alkanes.

In the charge-dipole interaction model, e.g. a combined EEM and PDI model^{58–63} or a combined capacitance model and PDI model,^{50,64–67} each atom is associated with both a net electric charge and a dipole. In the capacitance model, the charge-transfer term is determined in terms of the atomic capacitance which is the inverse of the atomic chemical hardness. Frequency-dependent polarizabilities have been calculated by the charge-dipole interaction model, where the interaction with oscillating electric fields are considered by including the kinetic energy of the atomic charges and the atomic dipoles^{68–71} and it has been extended to the calculation of absorption spectra.^{72,73}

In this work, frequency-dependent polarizabilities have been parametrized by a combined charge-transfer and point-dipole interaction (CT-PDI) model,^{74,75} where the charge-transfer and dipole terms are obtained using the AACT and PDI models, respectively, and the charge-dipole interaction gives the coupling between the two models. An extra energy term is added to the charge-transfer term in our model to obtain polarizabilities that scale correctly with the size of the system. One set of atom-type parameters is used for each element which can be determined assuming that the amount of charge-transfer in a bond is a function of the bond distance.⁵⁷

Solving the CT-PDI model, or any similar model, for the frequency-dependent polarizability gives direct information about the local electric fields as the response to an external electric field (both static and optical frequency). In the calculation of local electric fields, it is in most cases of interest to locate “hot spots”, i.e. points where the local field is very high which can initiate rare events in chemistry. As an example where static fields are important, in electrical breakdown in insulating liquids,⁷⁶ the probability of the production of free electrons increases at the location of high local electric fields. In this context, we have developed a model for calculating the field-dependent ionization potential,^{77–80} but the local field is

needed to deduce the actual molecular ionization potential in an electrically insulating liquid.

Local electric fields at optical frequencies play a role in many other phenomena. For aggregates of molecules they determine the interactions between molecules that lead to exciton transport and shifts in excited state energies. For molecules in solvents they are responsible for the solvent-induced effects on optical spectra. In addition, they are important in surface-enhanced Raman scattering (SERS),^{81–84} where the local field near metal nanoparticles is enhanced by plasmon excitation. Indeed, previously there have been calculations of electric fields in the vicinity of silver clusters as models of SERS.^{85,86} However, metal clusters or particles are not required in order to generate observable effects. For example, solvent vibrational modes have been observed in the resonance Raman and resonance HyperRaman spectra of small molecules.^{87,88} In addition, there is much current interest in the plasmonic states of aromatic molecules,^{89,90} where one expects to see enhanced fields and hot spots.

Previously, the CT-PDI model was used to calculate the frequency-dependent polarizability.^{74,75} In this work, the CT-PDI model is parametrized against TDDFT calculations and is applied to two molecular dimers, benzene and azobenzene, where the local field response to the frequency-dependent external electric field is calculated for frequencies through the first absorption maximum. Since the emphasis in this work is on method development and testing by comparisons with TDDFT, only simple dimer structures are considered. However the methods we are developing have the capability of being applied to much larger systems, including molecular aggregates and large graphene-like aromatic systems.

2 Theory

In this work, a force-field model for the response of the local electric field to the external field (local field factor) is presented. In our model, the local electric field at atom I , $E_{I,\beta}^{\text{loc}}$, is the sum of the external electric field, $E_{I,\beta}^{\text{ext}}$, and a field from the surrounding atoms, $E_{I,\beta}^{\text{pol}}$,

$$E_{I,\beta}^{\text{loc}} = E_{I,\beta}^{\text{ext}} + E_{I,\beta}^{\text{pol}} \quad (1)$$

where Greek subscripts denote the Cartesian coordinates, x , y , or z , respectively.

The polarization field at atom I arises from the charges and dipole moments of the surrounding atoms

$$E_{I,\beta}^{\text{pol}} = \sum_{J \neq I}^N T_{IJ,\beta}^{(1)} q_J + T_{IJ,\beta\gamma}^{(2)} \mu_{J,\gamma} \quad (2)$$

where the Einstein summation convention is used for repeated subscripts. q_J is the atomic charge, $\mu_{J,\gamma}$ is the atomic dipole

moment. Here, q_J and $\mu_{J,\gamma}$ includes both permanent contributions (from that the isolated molecule has a permanent dipole and/or quadrupole moment) and induced contributions from the electric field of the surroundings. In our model, Gaussian charge distributions for each atom are adopted instead of point-charges.^{49,91} The electrostatic energy between two Gaussian charge distributions is

$$V_{IJ} = q_I q_J \frac{\text{erf}(\sqrt{a_{IJ}} R_{IJ})}{R_{IJ}} \quad (3)$$

where R_{IJ} is the distance between atoms I and J , and a_{IJ} is

$$a_{IJ} = \frac{\phi_I \phi_J}{\phi_I + \phi_J} \quad (4)$$

where ϕ_I is an atom-type parameter describing the width of the Gaussian distribution. The relatively complex form of the error function can be approximated as^{91,92}

$$V_{IJ} = \frac{q_I q_J}{\sqrt{R_{IJ}^2 + \frac{\pi}{4a_{IJ}}}} \quad (5)$$

where the limiting behaviour at $R_{IJ} \rightarrow 0$ and $R_{IJ} \rightarrow \infty$ in equation 3 is retained.

In the same way, the electrostatic interaction between a point charge q_P and a Gaussian charge distribution of atom I is given as

$$V_{PI} = \frac{q_I q_P}{\sqrt{R_{PI}^2 + \frac{\pi}{4\phi_I}}} \quad (6)$$

Therefore, the local field factor at atoms are given with the electrostatic damping in equation 5 and at other points in space equation 6 is applied, respectively.

$T_{IJ,\beta}^{(1)}$ and $T_{IJ,\beta\gamma}^{(2)}$ in equation 2 are the charge-dipole and dipole-dipole interaction tensors

$$T_{IJ,\beta}^{(1)} = \nabla_\beta \frac{1}{\tilde{R}_{IJ}} = \frac{-R_{IJ,\beta}}{\tilde{R}_{IJ}^3} \quad (7)$$

and

$$T_{IJ,\beta\gamma}^{(2)} = \nabla_\gamma T_{IJ,\beta}^{(1)} = \frac{3R_{IJ,\beta} R_{IJ,\gamma} - \delta_{\beta\gamma} \tilde{R}_{IJ}^2}{\tilde{R}_{IJ}^5} \quad (8)$$

where $R_{IJ,\beta} = R_{I,\beta} - R_{J,\beta}$, $R_{I,\beta}$ is the coordinate of atom I and $\tilde{R}_{IJ} = \sqrt{R_{IJ}^2 + \frac{\pi}{4a_{IJ}}}$. In our model, the atomic charge is replaced by the charge-transfer term, q_{JM} .^{49,57}

$$q_J = \sum_M^N q_{JM} \quad (9)$$

Inserting equation 9 into equation 2 gives the local field in terms of the charge-transfer variables instead of atomic charges,

$$E_{I,\beta}^{\text{pol}} = \sum_{J \neq I, M > J}^N (T_{IJ,\beta}^{(1)} - T_{IM,\beta}^{(1)}) q_{JM} + \sum_{J \neq I}^N T_{IJ,\beta\gamma}^{(2)} \mu_{J,\gamma} \quad (10)$$

where we have used that $q_{MJ} = -q_{JM}$. In the CT-PDI model, the molecular polarizability for a homogenous external field, $E_{I,\alpha}^{\text{ext}} = E_\alpha^{\text{ext}}$, is given as⁵⁷

$$\alpha_{\gamma\alpha} = \sum_{J, M > J}^N R_{JM,\gamma} \frac{\partial q_{JM}}{\partial E_\alpha^{\text{ext}}} + \sum_J^N \frac{\partial \mu_{J,\gamma}}{\partial E_\alpha^{\text{ext}}} \quad (11)$$

where $\partial q_{JM} / \partial E_\alpha^{\text{ext}}$ is the charge-transfer contribution to the polarizability and $\partial \mu_{J,\gamma} / \partial E_\alpha^{\text{ext}}$ is the dipole contribution to the polarizability. $\partial q_{JM} / \partial E_\alpha^{\text{ext}}$ and $\partial \mu_{J,\gamma} / \partial E_\alpha^{\text{ext}}$ are calculated by solving a set of linear response equations for the frequency-dependent polarizability originating from minimizing a Lagrangian involving kinetic energies for the atomic charges and atomic dipole moments.^{69,74} A detailed presentation of the model for the calculation of the frequency-dependent polarizability can be found in Ref. 74.

The response of the local field to the external field becomes

$$\frac{\partial E_{I,\beta}^{\text{loc}}}{\partial E_\alpha^{\text{ext}}} = \delta_{\beta\alpha} + \sum_{J \neq I, M > J}^N (T_{IJ,\beta}^{(1)} - T_{IM,\beta}^{(1)}) \frac{\partial q_{JM}}{\partial E_\alpha^{\text{ext}}} + \sum_{J \neq I}^N T_{IJ,\beta\gamma}^{(2)} \frac{\partial \mu_{J,\gamma}}{\partial E_\alpha^{\text{ext}}} \quad (12)$$

i.e. it is given by the interaction tensors in equations 7 and 8 as well as the solutions to the response problem for the polarizability.

3 Model parametrization

The static and frequency-dependent polarizabilities are calculated using the TDDFT method^{6,93,94} with the PBE functional⁹⁵ and the augmented TZP basis set.^{96,97} The optimized geometries are obtained using the PBE functional and the TZP basis set.⁹⁶ Since dissipation is included in the CT-PDI model, it is also included in the quantum chemical calculations of the frequency-dependent polarizability.^{98,99} The life-time of the excited states is chosen to be 0.004 a.u in the TDDFT calculations. Thus, both the imaginary and the real part of the polarizabilities are calculated. The ADF software^{100,101} is applied in all the DFT calculations.

The TDDFT polarizabilities are used as reference data for the parametrization of the CT-PDI model. The first $\pi \rightarrow \pi^*$ excitation of azo dyes, aromatic molecules and polyenes as well as the first $\sigma \rightarrow \sigma^*$ excitation of alkanes are included in the parametrization, while higher excitations are ignored. The set of azobenzenes studied in our previous work⁷⁵ is here extended by a set of hydrocarbons. The parameters were optimized by a simplex algorithm to minimize the relative root mean square deviation (RMSD) between the polarizabilities

Table 1 Atom-type parameters (a.u.) of the CT-PDI model with a brief description. The corresponding equations can be found in Ref 74.

	description	C	H	N
α	isotropic atomic polarizability	8.2569	2.5564	4.8957
x	anisotropic atomic polarizability	0.2576	0.5021	0.2874
η	chemical hardness	2.7742	2.9595	3.1935
ϕ	width of a Gaussian distribution	1.2193	0.4599	2.6465
g_0	charge-transfer in non-metallic systems	0.7765	0.2052	1.0624
g_1	charge-transfer in metallic systems	0.9964	0.2236	1.2355
C	steepness of the charge-transfer	1.7372	2.1490	4.9503
R	atomic radius	1.3947	0.7516	1.1708
c_q	number of oscillating charges	3.1893	3.8734	1.1866
c_μ	number of oscillating dipoles	0.1222	2.3579	4.1181
γ_q	dissipation of charge	0.0121	0.0210	0.0033
γ_μ	dissipation of dipole	0.0127	0.0226	0.0018

calculated by the TDDFT method and the CT-PDI model. Both the real and the imaginary part of the full polarizability tensor are parametrized.

The values of the parameters are presented in table 1 with a brief description and table 2 presents the molecules grouped as a training set for the parametrization and a validation set to evaluate the parameters. The equations including all parameters can be found in Ref. 74 and are not repeated here. α and x are the isotropic and anisotropic atomic polarizability parameters, respectively, describing the atomic polarizability. η is the chemical hardness parameter in the regular EEM and the width of a Gaussian charge distribution is described by the ϕ parameter. To describe the non-metallic behaviour, a charge-transfer model is introduced that contains four atom-type parameters, g_0 , g_1 , C and R . Also four atom-type parameters, c_q , c_μ , γ_q and γ_μ are used to describe the frequency-dependence. More specifically, c_q and c_μ correspond the inverse of the number of oscillating charges and dipoles, respectively, whereas γ_q and γ_μ describe the dissipation of the charge and dipole contributions, respectively.

The obtained values of the parameters are in some cases different from our previous work.⁷⁵ The largest change is in the c_q and c_μ parameters. The c_q parameter of the hydrogen atom decreases from 6.1514 a.u.⁷⁵ to 3.8734 a.u. in this work, while c_μ increases from 0.6823 to 2.3579 a.u. indicating that for hydrogen the contribution from oscillating dipole moments decreases whereas the oscillating charge-transfer increases in importance. The reason for these discrepancies between the new and old parameters is that here we provide parameters for a wider set of molecules including a set of hydrocarbons in addition to the azo dyes in our previous work.⁷⁵ It is an ambitious goal to have a single set of atom-type parameters for carbon with the different properties of alkanes, aromatic systems, polyenes and polyynes, but we believe that the CT-PDI model^{74,75} is a step in the right direction. The instability of the parameter values is a common phenomenon especially in charge equilibration models, and there is no agreement on a

generic set of optimal parameters.¹⁰² To provide a comprehensive model that can describe an extensive set of molecular systems, the parameters still need to be improved. The goal is to extend the set of molecules step by step but provide a single set of parameters for all included molecules rather than system-specific parameter sets. Also it is desirable to have atom-type parameters and not for example bond and three-body parameters, as well as only have one set of parameters for each element. Further developments of the model should rather be in the direction of improving the physics of each term by including for example higher-order terms such as atomic quadrupole moments and atomic hyperpolarizabilities.

The excitation energies and the static polarizabilities calculated by the TDDFT and CT-PDI models are shown in table 2 as well as experimental values. The $\pi \rightarrow \pi^*$ excitation energies of the azo dyes calculated by the CT-PDI model are in good agreement with the TDDFT method. The largest error is around 15 % for 2,4,6-tricyano-4'-diethylaminoazobenzene in the validation set. Among the aromatic molecules, benzene, toluene and aniline, the largest error of the $\pi \rightarrow \pi^*$ excitation energy is 19 % for toluene. The CT-PDI model overestimates the shift in the excitation energy when a methyl substituent is added to a phenyl ring of benzene (e.g. toluene) compared to the TDDFT method and the experimental value.

In the case of polyenes, the errors are larger for the longer chains, $C_{14}H_{16}$, $C_{18}H_{20}$ and $C_{22}H_{24}$ compared to the shorter one, C_4H_6 . For polyenes the shift in the excitation energy with increasing the chain length is in good agreement with the TDDFT method. The $\sigma \rightarrow \sigma^*$ excitation energy of alkanes is in good agreement with the TDDFT method and also the excitation energy shift is predicted well by the CT-PDI model. The CT-PDI excitation energies are in good agreement with the experimental values and the deviations arise from solvent effects in the experiments.

The errors in the static polarizability of azo dyes are comparable to our previous work⁷⁵ and in some cases it is smaller. For example, 2,4,6-tricyano-4'-diethylaminoazobenzene has the largest error of the static polarizability 23 % in our previous work, while here it is 1 %. For the alkanes, the static polarizability is in good agreement with TDDFT. The largest error is 17 % in ethane, while in dodecane it is only 0.85 %. The CT-PDI model also gives the static polarizability of aromatic molecules in good agreement with the TDDFT method. The static polarizability of polyenes shows the largest error around 31 % for $C_{22}H_{24}$.

Fig. 1 shows the carbon-carbon bond distance distribution of the molecules in the training set. As could be expected, the model works better for the bond distances with higher probabilities which is due to that our non-metallic correction to the charge-transfer model strongly depends on the bond distances. The highest peak around 1.40 Å shows the distribution of aromatic bonds, whereas the second highest peak around 1.53 Å

Table 2 The excitation energy (eV) and static polarizability (a.u.) calculated by the TDDFT and CT-PDI models.

	molecule	Excitation Energy				Static Polarizability			
		TDDFT	CT-PDI	Error %	Exp.	TDDFT	CT-PDI	Error %	Exp.
training set	<i>trans</i> -azobenzene	3.37	3.32	1.48	3.90 ¹⁰³	198.7	201.8	1.56	171.4 ¹⁰⁴
	3-methylazobenzene	3.40	3.27	3.82	3.85 ¹⁰³	215.5	226.7	5.20	
	4-methylazobenzene	3.27	3.18	2.75	3.72 ¹⁰³	220.8	224.7	1.77	
	4-aminoazobenzene	2.99	3.13	4.68	3.19 ¹⁰⁵	232.4	226.4	2.58	
	4-cyanoazobenzene	2.99	3.20	7.02	3.81 ¹⁰⁵	233.0	242.5	4.08	
	4,4'-di-diethylaminoazobenzene	2.53	2.88	13.80	2.91 ¹⁰⁶	432.6	377.3	12.78	
	4-methyl-4'-dimethylaminoazobenzene	2.76	3.02	9.42	3.05 ¹⁰⁷	297.6	290.0	2.55	
	4,4'-diaminoazobenzene	2.80	3.05	8.93		264.9	249.3	5.89	
	benzene	6.80	6.26	7.94	6.20 ¹⁰⁸	70.9	72.0	1.55	70.1 ¹⁰⁹
	toluene	6.53	5.28	19.14	5.76 ¹¹⁰	85.5	92.1	7.72	82.7 ¹⁰⁹
	1,3-butadiene (C ₄ H ₆)	5.39	4.95	8.16	5.92 ¹¹¹	58.9	51.0	13.41	54.7 ¹¹²
	1,3,5,7,9,11,13-tetradecaheptaene (C ₁₄ H ₁₆)	2.61	2.01	22.99		349.3	296.1	15.23	
	ethane	8.11	8.16	0.61	8.70 ¹¹³	30.4	25.2	17.10	30.2 ¹⁰⁹
	propane	7.56	7.59	0.40	8.10 ¹¹³	43.4	37.6	13.36	42.4 ¹⁰⁹
	<i>n</i> -tridecane	7.35	7.02	4.49		535.4	543.1	1.44	
	cyclohexane	7.40	7.51	1.49	7.00 ¹¹⁴	75.3	72.6	3.59	74.2 ¹⁰⁹
	validation set	2-methylazobenzene	3.27	3.54	8.26		213.4	218.9	2.58
4-dimethylaminoazobenzene		2.79	2.99	7.17	3.07 ¹⁰⁷	274.5	265.7	3.21	
4-diethylaminoazobenzene		2.75	3.05	10.91	2.99 ¹⁰³	312.6	290.4	7.10	
4-cyano-4'-dimethylaminoazobenzene		2.67	2.90	8.61	2.75 ¹¹⁵	328.9	306.6	6.78	
4,4'-dimethylazobenzene		3.24	3.13	3.40		242.5	251.6	3.75	
4-amino-4'-methylazobenzene		2.98	3.09	3.69		252.5	250.5	0.79	
4,4'-di-dimethylaminoazobenzene		2.60	2.94	13.08	2.94 ¹¹⁶	352.3	327.7	6.98	
4-cyano-4'-diethylaminoazobenzene		2.58	2.86	10.85	2.66 ¹¹⁷	362.9	331.1	8.78	
2,4,6-tricyano-4'-diethylaminoazobenzene		2.48	2.86	15.32	2.21 ¹¹⁷	401.4	395.9	1.37	
aniline		4.35	4.24	2.53	4.40 ¹¹⁰	84.5	88.3	4.50	78.1 ¹⁰⁹
1,3,5,7,9,11,13,15,17-Octadecanonaene (C ₁₈ H ₂₀)		2.18	1.80	17.43		539.5	413.0	23.45	
1,3,5,7,9,11,13,15,17,19,21-Docosaundecaene (C ₂₂ H ₂₄)		1.90	1.66	12.63		770.6	532.9	30.85	
octane		6.80	7.07	3.97	7.50 ¹¹³	110.0	107.0	2.73	104.2 ¹⁰⁹
dodecane		7.35	7.02	4.49		164.7	166.1	0.85	153.5 ¹⁰⁹

shows the bond distance distribution of single C-C bonds. The small peaks around 1.35 Å represent the bonds in polyenes and the small peak around 1.50 Å shows the carbon bond of a methyl group bound to a phenyl ring as for example in toluene. In general, the molecules with the largest errors in table 2 can be explained by their small contribution to the bond distance distribution in the training set. The charge-transfer model in CT-PDI has a strong bond-distance dependence and is based on the sum of the two distances between three connected atoms in a molecule ($R_{IJ} + R_{JK}$, $I \neq K$)⁵⁷ (the variation of the sum of the two distances is an order of magnitude smaller than the variation of the individual bond distances). In the molecules with methyl substituents, e.g. toluene, the sum of the two bond distances between the carbon atoms of the methyl group and phenyl ring is around 2.9 Å, and the charge-transfer through this bond is not well described which leads to the relatively large error in the frequency-dependent polarizability. Since the $\pi \rightarrow \pi^*$ excitation in azo dyes is caused by the dipole term in the azo group and the adjacent carbon atoms,⁷⁵ the excitation energy in azobenzenes with methyl substituents is still well predicted because the charge-transfer in the phenyl-methyl bonds do not contribute substantially. The same problem appears for polyenes with the sum of the two distances around 2.7 Å in a π -conjugated chain of carbon atoms, which is not well represented in the parametrization.

Fig. 2 shows the frequency-dependent isotropic polarizabil-

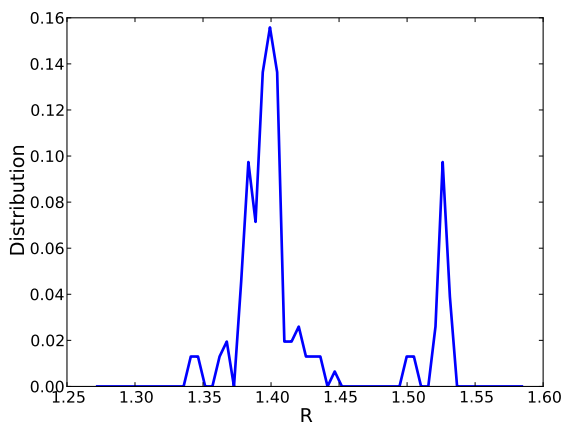


Fig. 1 The carbon-carbon bond distance (Å) distribution of the molecules in the training set.

ity of some of the molecules in the training set (left) and in the validation set (right) as well as their charge and dipole contributions. The maximum of the imaginary part of the polarizability gives the absorption frequency. Although the absorption frequencies calculated by the CT-PDI model are in good agreement with the TDDFT method, the polarizabilities at the absorption frequency are in some cases smaller than the TDDFT polarizabilities which affects the local field factor at the absorption frequency. The dipole term dominates the charge term for all the molecules but at the absorption frequency, the charge and dipole terms become comparable especially in the case of azo dyes and long polyenes.

4 Results and discussion

The local field response to the external field is calculated for two dimers, the benzene dimer and the *trans*-azobenzene dimer. The relative orientation of the dimers as well as the definition of the coordinate system are given in Fig. 3. Although not optimized dimers structures, the chosen structures give a good indication of the magnitude of the local field factors. It is important that the dimers are placed along one of the axes, here the *x*-axis, since, as discussed below, the response is larger for a field along a chain of molecules. The two molecules are in the training set and the CT-PDI model predicts their frequency-dependent polarizabilities in good agreement with TDDFT. At the absorption frequency, the CT-PDI polarizability of benzene is smaller than for TDDFT leading to that the calculated local field factor of the benzene dimer at the absorption frequency is underestimated by the CT-PDI model as compared to TDDFT. The local field factor is calculated at a point between the monomers (at the origin of the coordinate system shown in Fig. 3) and at the atoms for different distances between the monomers. Results are presented for frequencies through the $\pi \rightarrow \pi^*$ absorption frequency for atoms with large responses and two intermolecular distances are chosen to study the distance dependence of the local field factor. The minimum distance is chosen to prevent van der Waals strain between the hydrogen atoms of monomers. Therefore, the distance between the hydrogen atoms (with a van der Waals radius of 1.09 \AA^{118}) of the monomers is longer than twice the radius.

4.1 Benzene dimer

Fig. 4 shows the local field response of the benzene dimer at the point between the monomers (at the origin of the coordinate system) and at one of the hydrogen atoms (number 16 in Fig. 3) at two intermolecular distances, 8 and 10 \AA (between the center of the benzene rings), in the *x*-direction of the external electric field. As expected both the static and the

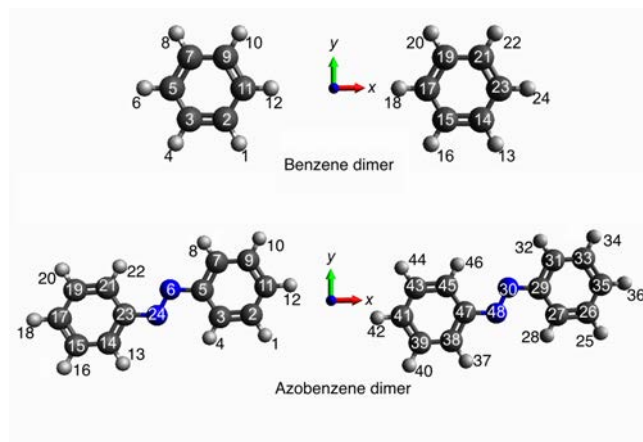


Fig. 3 The benzene and azobenzene dimers. The origin of the coordinate system for each dimer is shown at the point between the monomers.

frequency-dependent local field responses decrease with increasing distance. At 8 \AA , the static local field response at the point, $\partial E_{P,x}^{\text{loc}}/\partial E_x^{\text{ext}}$, is around 2 and at the absorption frequency it increases to around 4.5, while at 10 \AA it increases from around 1.5 to around 2.5 at the absorption frequency. The local field responses $\partial E_{P,y}^{\text{loc}}/\partial E_x^{\text{ext}}$ and $\partial E_{P,z}^{\text{loc}}/\partial E_x^{\text{ext}}$ are zero for symmetry reasons. At hydrogen atom 16 (see Fig. 3), $\partial E_{I,y}^{\text{loc}}/\partial E_x^{\text{ext}}$ is larger than $\partial E_{I,x}^{\text{loc}}/\partial E_x^{\text{ext}}$ and the responses are less dependent on the intermolecular distance compared to the local field factor at the point between the dimers. The response, $\partial E_{I,y}^{\text{loc}}/\partial E_x^{\text{ext}}$, is 0.9 at zero frequency and 3.5 at the absorption frequency, respectively, while $\partial E_{I,x}^{\text{loc}}/\partial E_x^{\text{ext}}$ is 0.6 at zero frequency and -0.5 at the absorption frequency, respectively. The dipole contribution dominates over the charge contribution at the frequencies below the absorption, while they are comparable at the absorption frequency.

Fig. 5 shows the local field response at carbon atom 2 and hydrogen atom 12 at 8 \AA in the *x*-direction of the external electric field. The charge term at carbon atom 2 cancels to a large extent the dipole term at the absorption frequency leading to the small local field factor. At 8 \AA , the largest local field factor is at hydrogen atoms 12 and 18 which is 2.3 at zero frequency and 6.2 at the absorption frequency. The results show that at these atoms, not only $\partial E_{I,x}^{\text{loc}}/\partial E_x^{\text{ext}}$ increases with frequency but also $\partial E_{I,y}^{\text{loc}}/\partial E_y^{\text{ext}}$ increases from around 0 to 3.15 at the absorption frequency.

The local field response at the atoms show that the response at the hydrogen atoms increases more significantly than at the carbon atoms due to a cancellation of the charge and dipole terms at the carbon atoms. $\partial E_{I,x}^{\text{loc}}/\partial E_y^{\text{ext}}$ and $\partial E_{I,y}^{\text{loc}}/\partial E_x^{\text{ext}}$ at the carbon and hydrogen atoms increase from 0.1 and 0.9 to 0.6 and 3.7, respectively, except for the atoms on the *x*-

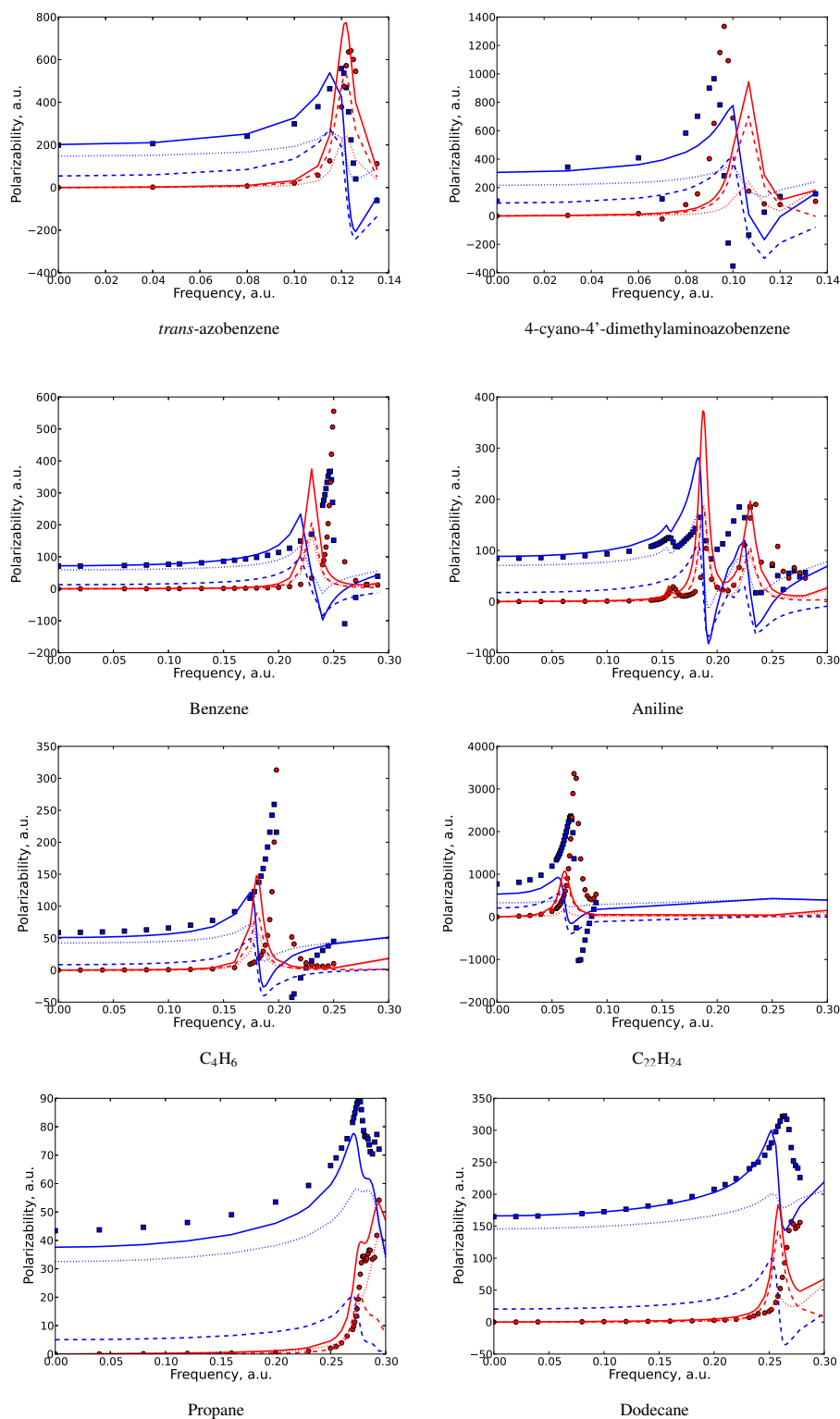


Fig. 2 The isotropic polarizability of the molecules in the training set (left) and validation set (right). The solid lines show the polarizability calculated by the CT-PDI model. The squares and circles show the TDDFT calculations. The dashed line is the charge, and the dotted line is the dipole contribution of the polarizability, respectively. The blue and red colors show the real and imaginary part of the polarizability, respectively. (1 a.u. = 27.21 eV)

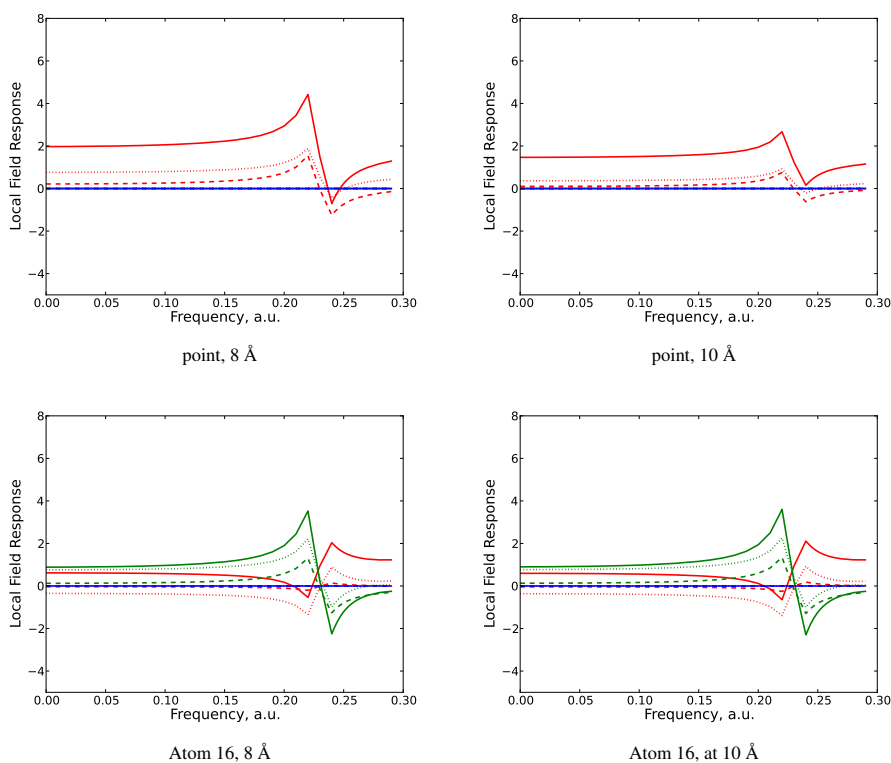


Fig. 4 The local field response of the benzene dimer at a point between the monomers and carbon atom 16 in the x -direction of the external electric field at the intermolecular distances of 8 and 10 Å. The red line is $\frac{\partial E_{I_x}^{\text{loc}}}{\partial E_x^{\text{ext}}}$, the green and blue lines are $\frac{\partial E_{I_y}^{\text{loc}}}{\partial E_x^{\text{ext}}}$ and $\frac{\partial E_{I_z}^{\text{loc}}}{\partial E_x^{\text{ext}}}$, respectively. The dashed line is the charge contribution and the dotted line is the dipole contribution, respectively. (1 a.u. = 27.21 eV)

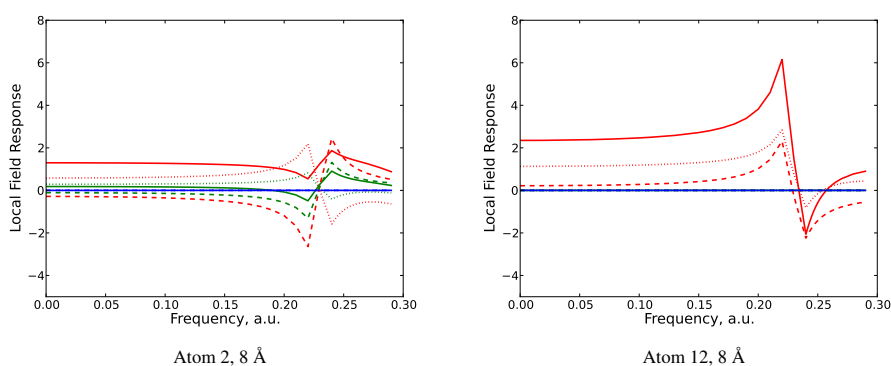


Fig. 5 The local field response of the benzene dimer at carbon atom 2 and hydrogen atom 12 in the x -direction of the external electric field at the intermolecular distance of 8 Å. The red line is $\frac{\partial E_{I_x}^{\text{loc}}}{\partial E_x^{\text{ext}}}$, the green and blue lines are $\frac{\partial E_{I_y}^{\text{loc}}}{\partial E_x^{\text{ext}}}$ and $\frac{\partial E_{I_z}^{\text{loc}}}{\partial E_x^{\text{ext}}}$, respectively. The dashed line is the charge contribution and the dotted line is the dipole contribution, respectively. (1 a.u. = 27.21 eV)

direction where these two responses are zero because of symmetry reasons. In general, the local field factor of the benzene dimer is large at the hydrogen atoms in the direction of the external electric field as well as at a point between monomers as compared to at the carbon atoms which is explained by if the charge and dipole terms add up or to a large extent cancel each other.

4.2 Azobenzene dimer

Fig. 6 shows the local field response of the azobenzene dimer at a point between the monomers (at the origin of the coordinate system shown in Fig. 3) and at carbon atom 11 in the x -direction of the external electric field at the intermolecular distances 13 and 15 Å (between the center of the azo bonds in the monomers). At the point between the dimers, the local field response at 13 Å, $\partial E_{P,x}^{\text{loc}}/\partial E_x^{\text{ext}}$, is 3.3 at zero frequency, while it is around 7 at the absorption frequency. At 15 Å, it only increases from around 2 at zero frequency to around 4 at the absorption frequency. At carbon atom 11, $\partial E_{I,x}^{\text{loc}}/\partial E_x^{\text{ext}}$ is 1.8 at zero frequency and it increases to 5.4 at the absorption frequency, while $\partial E_{I,y}^{\text{loc}}/\partial E_x^{\text{ext}}$ increases from around 0.1 at zero frequency to 2.3 at the absorption frequency. The charge term adds up to the dipole term giving rise to a larger local field factor as compared to the carbon atoms in the benzene dimer where the charge and dipole terms to a large extent canceled each other. The charge contribution increases more significantly at the absorption frequency compared to the dipole contribution as was the case also for the benzene dimer.

Fig. 7 (left) shows the largest local field response of the azobenzene dimer at 13 Å (in a scale different from the other figures). $\partial E_{I,x}^{\text{loc}}/\partial E_x^{\text{ext}}$ at the nitrogen atoms in the azo groups are around 4.5 at zero frequency and 12 at the absorption frequency. $\partial E_{I,y}^{\text{loc}}/\partial E_x^{\text{ext}}$ increases from 2 at zero frequency to around 10 at the absorption frequency. At the nitrogen atoms, the dipole term gives the major contribution to the local field factor whereas the contribution of the charge term is small. The second largest local field response is at hydrogen atoms 12 and 42 where $\partial E_{I,x}^{\text{loc}}/\partial E_x^{\text{ext}}$ at zero frequency is around 3.2 and at the absorption frequency is 7.7 (see Fig. 7 (right)).

The local field response, $\partial E_{I,x}^{\text{loc}}/\partial E_x^{\text{ext}}$, is also large but with an opposite sign at carbon atoms 3, 21, 27 and 45, around -1.4 at zero frequency and -8 at the absorption frequency, where both the charge and dipole terms have the same sign (negative). The local field response $\partial E_{I,x}^{\text{loc}}/\partial E_x^{\text{ext}}$ at these atoms is smaller (around 1.8 and 3.5 at zero frequency and the absorption frequency, respectively) than $\partial E_{I,y}^{\text{loc}}/\partial E_x^{\text{ext}}$ again because of cancellation of the charge and dipole terms. Thus, in the azobenzene dimer the response on the carbon and hydrogen atoms are comparable while at the nitrogen atoms it is significantly larger. A large degree of cancellation of charge and dipole terms is found in many of the remaining carbon and

hydrogen atoms.

The azobenzene dimer shows in general larger static and frequency-dependent local field factors at the carbon and hydrogen atoms than the benzene dimer. An important feature of the CT-PDI model is the division into a charge and a dipole term which may add up to give a relatively large local field factor or the two terms may to a large extent cancel each other. The dependence on the distance between the dimers is significant, indicating for example that the molecular local field factors will vary substantially for a molecular liquid at normal and elevated temperatures and pressures. The model is presently used for dielectric liquids to determine the local field factor as well as the macroscopic polarization and thereby also the optical part of the dielectric constant is obtained by combining molecular dynamic simulations and a modified Lorentz-Lorenz approach developed for the PDI model.³¹

The local field factors at all atoms of a monomer in the benzene and azobenzene dimers are given in the supplementary material.

5 Conclusions

A method to calculate local field factors based on a classical polarization model is presented, and some initial results for the benzene and azobenzene dimers are presented. The response increases significantly at the absorption frequency compared to frequencies below absorption and the largest local field response at the absorption frequency is around 12 at the nitrogen atoms of the azobenzene dimer and around 6 at the hydrogen atoms of the benzene dimer. The presented method is a rapid alternative to quantum calculations for large systems and for a combination with molecular dynamics simulations where we need to average over many configurations.¹¹⁹ A major advantage of a force-field model is the division into different terms, each with a physical interpretation, in this case a charge and a dipole term. In addition to the local field factor, the present version of the CT-PDI model gives the first absorption maximum and the frequency-dependent polarizability. In the future this method will be useful for modeling the static and optical properties of much larger systems, including molecular aggregates sampled from molecular dynamics simulations.¹²⁰

6 Acknowledgments

ND and POÅ would like to acknowledge a research grant “Modeling of electrical pre-breakdown and breakdown phenomena in insulating liquids” (200631/560) from the Norwegian Research Council, ABB and Statnett and a grant of computer time (account nn2920k) from the NOTUR project. GCS acknowledges support from the Castl Center (Center for

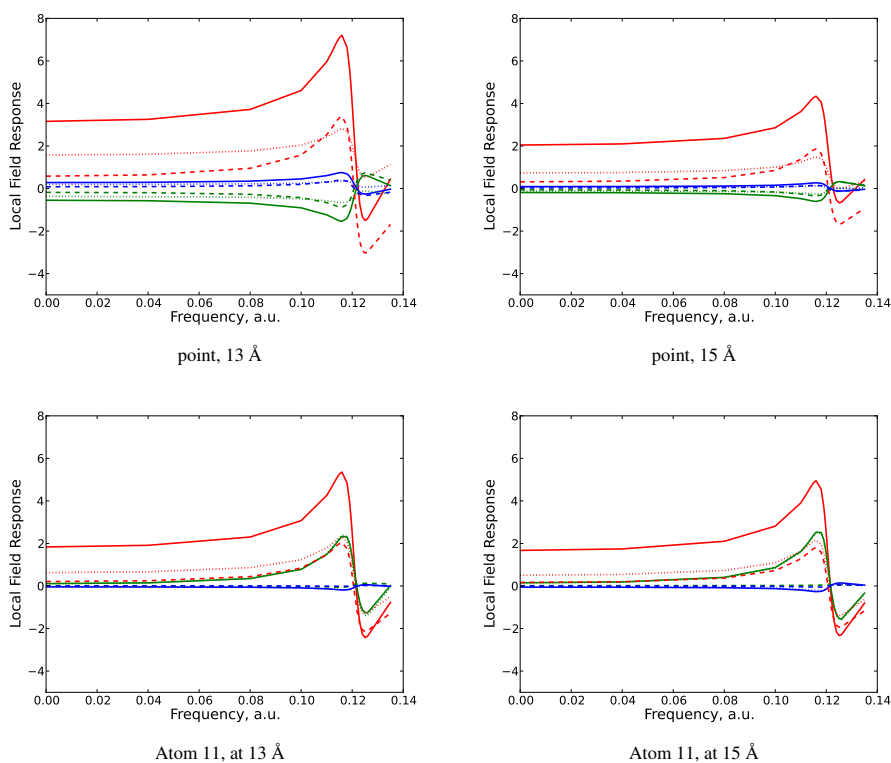


Fig. 6 The local field response of the azobenzene dimer at a point between monomers and carbon atom 11 in the x -direction of the external electric field at the intermolecular distances of 13 and 15 Å. The red line is $\frac{\partial E_{I_x}^{\text{loc}}}{\partial E_x^{\text{ext}}}$, the green and blue lines are $\frac{\partial E_{I_y}^{\text{loc}}}{\partial E_x^{\text{ext}}}$ and $\frac{\partial E_{I_z}^{\text{loc}}}{\partial E_x^{\text{ext}}}$, respectively. The dashed line is the charge contribution and the dotted line is the dipole contribution, respectively. (1 a.u. = 27.21 eV)

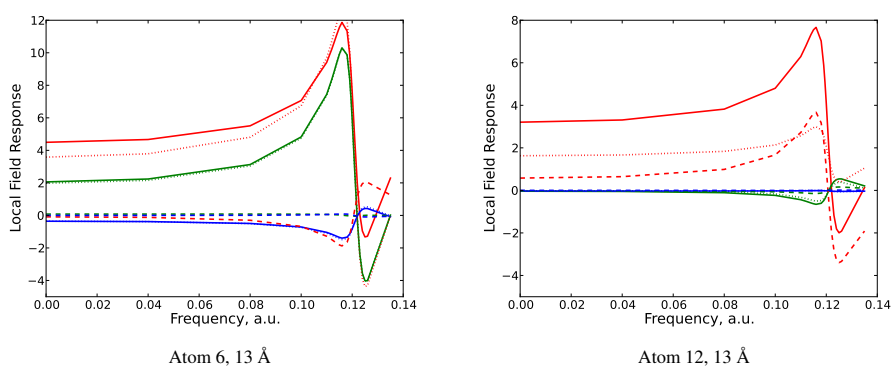


Fig. 7 The local field response of the azobenzene dimer at nitrogen atom 6 and hydrogen atom 12 in the x -direction of the external electric field at the intermolecular distances of 13 Å. The red line is $\frac{\partial E_{I_x}^{\text{loc}}}{\partial E_x^{\text{ext}}}$, the green and blue lines are $\frac{\partial E_{I_y}^{\text{loc}}}{\partial E_x^{\text{ext}}}$ and $\frac{\partial E_{I_z}^{\text{loc}}}{\partial E_x^{\text{ext}}}$, respectively. The dashed line is the charge contribution and the dotted line is the dipole contribution, respectively. (1 a.u. = 27.21 eV)

Chemistry at the Space-Time Limit). This is supported by the National Science Foundation, grant CHE-1414466. This project was initiated when POÅ was a one-year sabbatical at Northwestern University, which is acknowledged.

References

- 1 C. J. F. Böttcher, *Theory of Electric Polarization*, Elsevier, Amsterdam, Netherlands, 2nd edn, 1973, vol. 1.
- 2 J. D. Jackson, *Classical Electrodynamics*, John Wiley and Sons, New York, 2nd edn, 1975.
- 3 R. Wortmann and D. M. Bishop, *J. Chem. Phys.*, 1998, **108**, 1001–1007.
- 4 C. Kittel, *Introduction to solid state physics*, Wiley, New York, 4th edn, 1971.
- 5 J. Olsen and P. Jørgensen, *J. Chem. Phys.*, 1985, **82**, 3235–3264.
- 6 E. Runge and E. K. U. Gross, *Phys. Rev. Lett.*, 1984, **52**, 997–1000.
- 7 P. Lazzeretti, *Adv. Chem. Phys.*, 1987, **75**, 507–549.
- 8 P. Lazzeretti and R. Zanasi, *Chem. Phys. Lett.*, 1980, **71**, 529–533.
- 9 P. Lazzeretti and R. Zanasi, *Phys. Rev. A*, 1981, **24**, 1696–1704.
- 10 A. Soncini, P. Lazzeretti, V. Bakken and T. Helgaker, *J. Chem. Phys.*, 2004, **120**, 3142–3151.
- 11 C. V. Caillie and R. D. Amos, *Chem. Phys. Lett.*, 1998, **291**, 71–77.
- 12 S. J. A. van Gisbergen, J. G. Snijders and E. J. Baerends, *J. Chem. Phys.*, 1998, **109**, 10657–10668.
- 13 S. J. A. van Gisbergen, F. Kootstra, P. R. T. Schipper, O. V. Gritsenko, J. G. Snijders and E. J. Baerends, *Phys. Rev. A*, 1998, **57**, 2556–2571.
- 14 D. Guillaumont and S. Nakamura, *Dyes and Pigments*, 2000, **46**, 85–92.
- 15 N. T. Maitra and M. van Faassen, *J. Chem. Phys.*, 2007, **126**, 191106.
- 16 M. E. Casida and D. R. Salahub, *J. Chem. Phys.*, 2000, **113**, 8918–8935.
- 17 K. Burke, J. Werschnik and E. K. Gross, *J. Chem. Phys.*, 2005, **123**, 062206.
- 18 L. Jensen and N. Govind, *J. Phys. Chem. A*, 2009, **113**, 9761–9765.
- 19 M. A. Rohrdanz, K. M. Martins and M. Herbert, *J. Chem. Phys.*, 2009, **130**, 054112.
- 20 B. M. Wong and T. H. Hsieh, *J. Chem. Theory Comput.*, 2010, **6**, 3704–3712.
- 21 T. Körzdöfer, J. S. Sears, C. Sutton and J.-L. Brédas, *J. Chem. Phys.*, 2011, **135**, 204107.
- 22 L. Kronik, T. Stein, S. Rafaely-Abramson and R. Baer, *J. Chem. Theory Comput.*, 2012, **8**, 1515–1531.
- 23 H. Phillips, Z. Zheng, E. Geva and B. D. Dunietz, *Org. Electron.*, 2014, **15**, 1509–1520.
- 24 L. Silberstein, *Phil. Mag.*, 1917, **33**, 92–128.
- 25 L. Silberstein, *Phil. Mag.*, 1917, **33**, 521–533.
- 26 J. Applequist, J. R. Carl and K.-F. Fung, *J. Am. Chem. Soc.*, 1972, **94**, 2952–2960.
- 27 J. Applequist, *Acc. Chem. Res.*, 1977, **10**, 79–85.
- 28 K. A. Bode and J. Applequist, *J. Phys. Chem.*, 1996, **100**, 17820–17824.
- 29 L. Jensen, O. H. Schmidt, K. V. Mikkelsen and P.-O. Åstrand, *J. Phys. Chem. B*, 2000, **104**, 10462–10466.
- 30 L. Jensen, P.-O. Åstrand and K. V. Mikkelsen, *Nano Lett.*, 2003, **3**, 661–665.
- 31 L. Jensen, P.-O. Åstrand and K. V. Mikkelsen, *J. Phys. Chem. B*, 2004, **108**, 8226–8233.
- 32 M. Swart, J. G. Snijders and P. T. van Duijn, *J. Comput. Meth. Sci. Engin.*, 2004, **4**, 419–425.
- 33 L. Jensen, P.-O. Åstrand and K. V. Mikkelsen, *J. Phys. Chem. A*, 2004, **108**, 8795–8800.
- 34 M. van Faassen, L. Jensen, J. A. Berger and P. L. de Boeij, *Chem. Phys. Lett.*, 2004, **395**, 274–278.
- 35 J. Kongsted, A. Osted, L. Jensen, P.-O. Åstrand and K. V. Mikkelsen, *J. Phys. Chem. B*, 2001, **105**, 10243–10248.
- 36 T. Hansen, L. Jensen, P.-O. Åstrand and K. V. Mikkelsen, *J. Chem. Theory Comput.*, 2005, **1**, 626–633.
- 37 J. Applequist, *J. Chem. Phys.*, 1973, **58**, 4251–4259.
- 38 J. Applequist, *J. Am. Chem. Soc.*, 1973, **95**, 8258–8262.
- 39 K. R. Sundberg, *J. Chem. Phys.*, 1978, **68**, 5271–5276.
- 40 J. Applequist, *J. Phys. Chem. A*, 1998, **102**, 7723–7724.
- 41 K. R. Sundberg, *J. Chem. Phys.*, 1977, **66**, 114–118.
- 42 A. D. Buckingham, E. P. Concannon and I. D. Hands, *J. Phys. Chem.*, 1994, **98**, 10455–10459.
- 43 L. Jensen, K. O. Sylvester-Hvid, K. V. Mikkelsen and P.-O. Åstrand, *J. Phys. Chem. A*, 2003, **107**, 2270–2276.
- 44 L. Jensen, A. L. Esbensen, P.-O. Åstrand and K. V. Mikkelsen, *J. Comput. Meth. Sci. Engin.*, 2006, **6**, 353–364.
- 45 L. Jensen, P.-O. Åstrand and K. V. Mikkelsen, *J. Comput. Theor. Nanosci.*, 2009, **6**, 270–291.
- 46 W. J. Mortier, K. van Genechten and J. Gasteiger, *J. Am. Chem. Soc.*, 1985, **107**, 829–835.
- 47 A. K. Rappé and W. A. Goddard III, *J. Phys. Chem.*, 1991, **95**, 3358–3363.
- 48 H. A. Stern, G. A. Kaminski, J. L. Banks, R. Zhou, B. J. Berne and R. A. Friesner, *J. Phys. Chem. B*, 1999, **103**, 4730–4737.
- 49 R. Chelli, P. Procacci, R. Righini and S. Califano, *J. Chem. Phys.*, 1999, **111**, 8569–8575.
- 50 L. Jensen, P.-O. Åstrand and K. V. Mikkelsen, *Int. J. Quant. Chem.*, 2001, **84**, 513–522.
- 51 R. A. Nistor, J. G. Polihronov, M. H. Müser and N. J. Mosey, *J. Chem. Phys.*, 2006, **125**, 094108.
- 52 D. Mathieu, *J. Chem. Phys.*, 2007, **127**, 224103.
- 53 J. Chen and T. J. Martínez, *Chem. Phys. Lett.*, 2007, **438**, 315–320.
- 54 G. Lee Warren, J. E. Davis and S. Patel, *J. Chem. Phys.*, 2008, **128**, 144110.
- 55 J. Chen, D. Hundertmark and T. J. Martínez, *J. Chem. Phys.*, 2008, **129**, 214113.
- 56 R. A. Nistor and M. H. Müser, *Phys. Rev. B*, 2009, **79**, 104303.
- 57 H. S. Smalø, P.-O. Åstrand and L. Jensen, *J. Chem. Phys.*, 2009, **131**, 044101.
- 58 H. A. Stern, F. Rittner, B. J. Berne and R. A. Friesner, *J. Chem. Phys.*, 2001, **115**, 2237–2251.
- 59 A. Mayer, *Appl. Phys. Lett.*, 2005, **86**, 153110.
- 60 A. Mayer, *Phys. Rev. B*, 2005, **71**, 235333.
- 61 A. Mayer, P. Lambin and R. Langlet, *Appl. Phys. Lett.*, 2006, **89**, 063117.
- 62 A. Mayer, *Phys. Rev. B*, 2007, **75**, 045407.
- 63 A. Mayer and P.-O. Åstrand, *J. Phys. Chem. A*, 2008, **112**, 1277–1285.
- 64 M. L. Olson and K. R. Sundberg, *J. Chem. Phys.*, 1978, **69**, 5400–5404.
- 65 J. Applequist, *J. Phys. Chem.*, 1993, **97**, 6016–6023.
- 66 B. Shanker and J. Applequist, *J. Phys. Chem.*, 1994, **98**, 6486–6489.
- 67 L. L. Jensen and L. Jensen, *J. Phys. Chem. C*, 2008, **112**, 15697–15703.
- 68 L. Jensen, P.-O. Åstrand, K. O. Sylvester-Hvid and K. V. Mikkelsen, *J. Phys. Chem. A*, 2000, **104**, 1563–1569.
- 69 A. Mayer, P. Lambin and P.-O. Åstrand, *Nanotechnology*, 2008, **19**, 025203.
- 70 A. Mayer, A. L. González, C. M. Aikens and G. C. Schatz, *Nanotechnology*, 2009, **20**, 195204.
- 71 A. Mayer and G. C. Schatz, *J. Phys.: Condens. Matter*, 2009, **21**, 325301.
- 72 J. Applequist, K. R. Sundberg, M. L. Olson and L. C. Weiss, *J. Chem. Phys.*, 1979, **70**, 1240–1246.
- 73 B. Shanker and J. Applequist, *J. Chem. Phys.*, 1996, **104**, 6109–6116.

- 74 H. S. Smalø, P.-O. Åstrand and A. Mayer, *Mol. Phys.*, 2013, **111**, 1470.
- 75 Sh. Haghdani, N. Davari, R. Sandnes and P.-O. Åstrand, *J. Phys. Chem. A*, 2014, **118**, 11282–11292.
- 76 J. C. Devins, S. J. Rzd and R. J. Schwabe, *J. Appl. Phys.*, 1981, **52**, 4531–4545.
- 77 H. S. Smalø, Ø. Hestad, S. Ingebrigtsen and P.-O. Åstrand, *J. Appl. Phys.*, 2011, **109**, 073306.
- 78 N. Davari, P.-O. Åstrand, S. Ingebrigtsen and M. Unge, *J. Appl. Phys.*, 2013, **113**, 143707.
- 79 N. Davari, P.-O. Åstrand and T. Van Voorhis, *Mol. Phys.*, 2013, **111**, 1456–1461.
- 80 N. Davari, P.-O. Åstrand, M. Unge, L. E. Lundgaard and D. Linhjell, *AIP Adv.*, 2014, **4**, 037117.
- 81 H. Metiu, and P. Das, *Ann. Rev. Phys. Chem.*, 1984, **35**, 507–536.
- 82 M. Moskovits, *Rev. Mod. Phys.*, 1985, **57**, 783–826.
- 83 G. S. Kedziora and G. C. Schatz, *Spectrochim. Acta A*, 1999, **55**, 625–638.
- 84 M. Futamata, Y. Maruyama and M. Ishikawa, *J. Phys. Chem. B*, 2003, **107**, 7607–7617.
- 85 L. Zhao, L. Jensen and G. C. Schatz, *J. Am. Chem. Soc.*, 2006, **128**, 2911–2919.
- 86 L. Jensen, L. L. Zhao and G. C. Schatz, *J. Phys. Chem. C*, 2007, **111**, 4756–4764.
- 87 A. E. Johnson and A. B. Myers, *J. Phys. Chem.*, 1996, **100**, 7778–7788.
- 88 R. Shimada and H. Hamaguchi, *J. Chem. Phys.*, 2014, **140**, 204506.
- 89 E. B. Guidez and C. M. Aikens, *J. Phys. Chem. C*, 2013, **117**, 21466–21475.
- 90 A. Manjavacas, F. Marchesin, S. Thongrattanasiri, P. Koval, P. Nordlander, D. Sánchez-Portal and F. J. García de Abajo, *ACS Nano*, 2013, **7**, 3635–3643.
- 91 L. Jensen, P.-O. Åstrand, A. Osted, J. Kongsted and K. V. Mikkelsen, *J. Chem. Phys.*, 2002, **116**, 4001–4010.
- 92 G. A. van der Velde, *A realistic Coloumb potential. MD and MC on water*, CECAM, France, H. J. C. Berendsen edn, 1972.
- 93 E. K. U. Gross, J. F. Dobson and M. Petersilka, *Top. Curr. Chem.*, 1996, **181**, 81–172.
- 94 M. A. L. Marques and E. K. U. Gross, *Ann. Rev. Phys. Chem.*, 2004, **55**, 427–455.
- 95 J. P. Perdew, K. Burke and M. Ernzerhof, *Phys. Rev. Lett.*, 1996, **77**, 3865–3868.
- 96 E. van Lenthe, E. J. Baerends, C. F. Guerra, S. J. A. van Gisbergen, J. G. Snijders and T. Ziegler, *J. Comput. Chem.*, 2003, **24**, 1142–1156.
- 97 D. P. Chong, *Mol. Phys.*, 2005, **103**, 749–761.
- 98 P. Norman, D. M. Bishop, H. J. Aa. Jensen and J. Oddershede, *J. Chem. Phys.*, 2001, **115**, 10323–10334.
- 99 L. Jensen, J. Autschbach and G. C. Schatz, *J. Chem. Phys.*, 2005, **122**, 224115.
- 100 C. F. Guerra, J. G. Snijders, G. te Velde and E. J. Baerends, *Theor. Chem. Acc.*, 1998, **99**, 391–401.
- 101 G. te Velde, F. M. Bickelhaupt, E. J. Baerends, C. F. Guerra, S. J. A. van Gisbergen, J. G. Snijders and T. Ziegler, *J. Comput. Chem.*, 2001, **22**, 931–967.
- 102 T. Verstraelen, P. Bultinck, V. V. Speybroeck, P. W. Ayers, D. V. Neck and M. Waroquier, *J. Chem. Theory Comput.*, 2011, **7**, 1750–1764.
- 103 E. Sawicki, *Org. Chem.*, 1957, **22**, 915–919.
- 104 T. Halicioğlu and O. Sinanoğlu, *Ann. N. Y. Acad. Sci.*, 1969, **158**, 308–317.
- 105 H. H. Jaffé, S. J. Yeh and R. W. Gardner, *J. Mol. Struct.*, 1958, **2**, 120–136.
- 106 C. Haessner and H. Mustroph, *J. F. Prakt. Chem.*, 1987, **329**, 493–498.
- 107 L. M. Yagupolskij and L. Z. Gandel'sman, *Zh. Obshch. Khim.*, 1965, **35**, 1252–1262.
- 108 J. Lorentzon, P.-Å. Malmqvist, M. Fülischer and B. O. Roos, *Theor. Chim. Acta*, 1995, **91**, 91–108.
- 109 K. J. Miller, *J. Am. Chem. Soc.*, 1990, **112**, 8533–8542.
- 110 K. Kimura and S. Nagakura, *Mol. Phys.*, 1965, **9**, 117–135.
- 111 R. McDiarmid, *J. Chem. Phys.*, 1976, **64**, 514–521.
- 112 C. Van Caillie and R. D. Amos, *Chem. Phys. Lett.*, 2000, **328**, 446.
- 113 J. W. Au, G. Cooper, G. R. Burton, T. N. Olney and C. E. Brion, *Chem. Phys.*, 1993, **173**, 209–239.
- 114 L. W. Pickett, M. Muntz and E. M. McPherson, *J. Am. Chem. Soc.*, 1951, **73**, 4862–4865.
- 115 F. Gerson and E. Heilbronner, *Helv. Chim. Acta*, 1962, **45**, 42–50.
- 116 F. Gerson and E. Heilbronner, *Helv. Chim. Acta*, 1962, **45**, 51–59.
- 117 J. Griffiths and B. Roozpeikar, *J. Chem. Soc., Perkin Trans. 1*, 1976, 42–45.
- 118 R. S. Rowland and R. Taylor, *J. Phys. Chem.*, 1996, **100**, 7384–7391.
- 119 A. Osted, J. Kongsted, K. V. Mikkelsen, P.-O. Åstrand and O. Christiansen, *J. Chem. Phys.*, 2006, **124**, 124503.
- 120 N. Davari, C. D. Daub, P.-O. Åstrand and M. Unge, manuscript.